
LoopQ: Quantization for Recursive Transformers

Rui Fang
National Taiwan University
rfang@arbor.ee.ntu.edu.tw

Hsi-Wen Chen
National Taiwan University
hwchen@arbor.ee.ntu.edu.tw

Ming-Syan Chen
National Taiwan University
mschen@ntu.edu.tw

Abstract

Looped language models (LoopLMs) improve parameter efficiency by recursively reusing Transformer blocks, enabling deeper computation under a fixed model size. However, this reuse makes LoopLMs more fragile under post-training quantization (PTQ). We present the first systematic study of quantization in LoopLMs and identify three challenges: **distribution shift across roles**, **state reuse across loop transitions**, and **recursive error accumulation**. To address these challenges, we propose **LoopQ**, a loop-aware PTQ framework that preserves a shared quantized backbone while introducing lightweight adaptations. LoopQ combines activation scaling, selective transformation, cross-loop state alignment, and trajectory-aware optimization to reduce distributional mismatch within loops and error accumulation across loops. Experiments across seven benchmarks show that, under W4A4 quantization, LoopQ improves average downstream accuracy by 68.8% and reduces average perplexity by 87.7% compared with the strongest static PTQ baseline.

1 Introduction

Quantization robustness [1, 34, 38] is critical for efficient LLM deployment on resource-constrained devices [39]. Looped language models (LoopLMs) [3, 5, 8, 17, 21, 45] improve expressiveness under a fixed parameter budget by **recursively reusing shared Transformer blocks**, making them attractive for memory- and bandwidth-constrained settings [19, 20, 43]. However, existing LoopLMs mainly target full-precision inference, while most post-training quantization (PTQ) methods optimize layer-wise quantization error [2, 14, 18, 22, 32, 35, 37] without accounting for error propagation through recursively reused states.

This limitation is particularly problematic for LoopLMs, which are substantially more sensitive to quantization than comparable non-loop architectures [40]. In our preliminary experiments, directly applying PTQ to LoopLMs leads to performance drops exceeding 50%. Under the same parameter budget, quantized non-loop LLMs can even outperform higher-precision LoopLMs. This suggests that the benefits of parameter reuse in full-precision settings do not automatically transfer to quantized regimes, where recursive reuse can amplify quantization-induced errors.

Figure 1 illustrates this vulnerability through two coupled phenomena induced by quantizing recursive computation. First, the top-left panel shows that the same physical layer exhibits different normalized P99 activation ranges across loop passes, indicating that a single static quantization configuration cannot accommodate multiple loop-dependent regimes. Second, the bottom-left panel shows that quantization errors do not remain local. Instead, they grow as recursion proceeds and exhibit pronounced spikes at loop transitions, where the hidden state produced by one loop is passed to the next. These observations suggest that quantization in LoopLMs is governed by both per-layer distributional mismatch and recursive error accumulation.

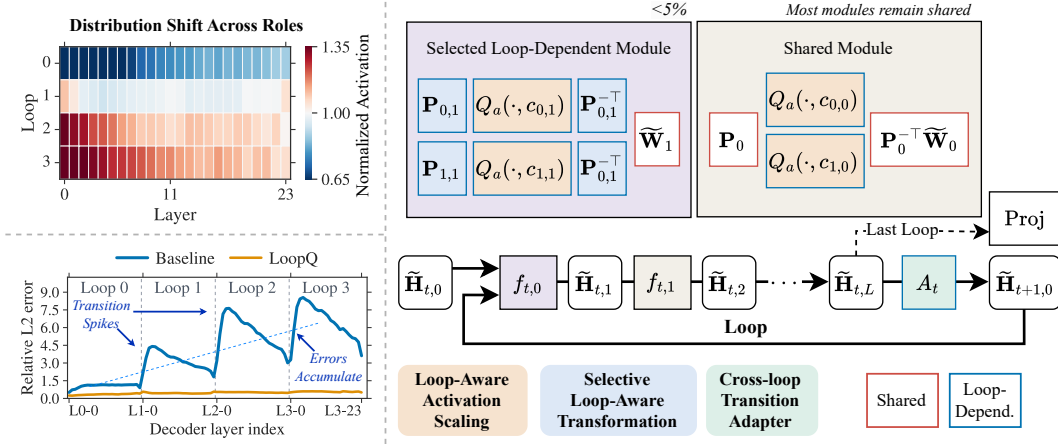


Figure 1: **Left:** LoopLMs exhibit loop-dependent activation drift (Challenge 1), error spikes at loop transitions (Challenge 2), and error accumulation across loops (Challenge 3). **Right:** LoopQ preserves a shared quantized backbone while adding lightweight loop-aware scaling, selective transformation, and cross-loop state alignment to reduce recursive quantization errors.

The root cause is that the same shared block is reused under different computational roles as recursion proceeds. A single physical layer therefore no longer behaves as a fixed feedforward position, but instead operates under stage-dependent roles across loops. This role variation leads to three key challenges, which we formalize through theoretical analysis: **(1) Distribution Shift across Roles**, where loop-dependent activation statistics cause scale and geometry mismatches under shared quantization; **(2) State Reuse across Transitions**, where the hidden state produced by one loop is reused as the input to the next, introducing transition inconsistency; and **(3) Recursive Error Accumulation**, where quantization errors propagate along the recurrent trajectory and are amplified by subsequent loop-dependent transformations.

A naive solution is to assign loop-specific quantization configurations to all loops, thereby fully adapting to loop-dependent distributions. However, this breaks the shared-parameter structure of recursive computation and introduces substantial memory and deployment overhead, undermining the efficiency advantages of LoopLMs. We therefore propose **LoopQ**, a loop-aware post-training quantization framework that preserves a shared quantized backbone while introducing lightweight loop-dependent adaptations that affect less than 5% of transformation parameters, corresponding to less than 0.12% of total model parameters.

As shown in the right panel of Figure 1, **Loop-aware Activation Scaling** (brown block) uses loop-dependent scales to track magnitude drift, while **Selective Loop-aware Transformation** (blue block) selectively introduces loop-dependent transforms for sharing-sensitive modules identified by *sharing-gap analysis*, correcting residual geometry mismatch. To stabilize loop transitions, **Cross-loop Transition Adapter** (green block) aligns cross-loop hidden states with a lightweight adapter. Finally, guided by fixed-point convergence [17], **Trajectory-Aware Calibration** performs progressive trajectory-aware calibration under the true recurrent dynamics to suppress trajectory-level error accumulation.

Our contributions are summarized as follows. (i) We provide the first systematic study of quantization in LoopLMs, identifying three foundational challenges in recursive computation: distribution shift across roles, state reuse across transitions, and recursive error accumulation. (ii) We propose LoopQ, a loop-aware post-training quantization framework that preserves a shared quantized backbone while introducing lightweight loop-dependent adaptations, including activation scaling, selective transformation, cross-loop state alignment, and trajectory-aware optimization. (iii) Experiments on seven benchmarks show that LoopQ outperforms five PTQ baselines, improving mean downstream accuracy by 68.8% and reducing average perplexity by 87.7% under W4A4 quantization.

2 Problem Formulation

We first introduce the LoopLM architecture, followed by the post-training quantization setting.

LoopLM. LoopLM is a recursive Transformer composed of a shared stack of L layers, applied iteratively for T loops. Let \mathbf{X} denote the input, and let $f_\ell(\cdot; \theta_\ell)$ represent the ℓ -th layer. We denote the hidden state at layer ℓ in loop t as $\mathbf{H}_{t,\ell} \in \mathbb{R}^{n \times d}$, where each row corresponds to a token representation. The initial state is $\mathbf{H}_{0,0} = \text{Embed}(\mathbf{X})$.

The loop computation is defined as

$$\mathbf{H}_{t,\ell} = f_\ell(\mathbf{H}_{t,\ell-1}; \theta_\ell), \quad \mathbf{H}_{t+1,0} = \mathbf{H}_{t,L}, \quad (1)$$

for $t \in \{0, \dots, T-1\}$ and $\ell \in \{1, \dots, L\}$. Let $\mathbf{H}_t := \mathbf{H}_{t,0}$. Each loop can be summarized by $F := f_L \circ \dots \circ f_1$, yielding $\mathbf{H}_{t+1} = F(\mathbf{H}_t)$, and the final output is $\mathbf{Z} = \text{Proj}(\mathbf{H}_T)$.

For analytical clarity, we express $f_\ell(\cdot; \theta_\ell)$ using a single weight matrix \mathbf{W}_ℓ , i.e., $\mathbf{H}_{t,\ell} = \mathbf{H}_{t,\ell-1} \mathbf{W}_\ell^\top$. This abstraction naturally extends to general Transformer blocks with multiple weight matrices.

Post-training Quantization on LoopLMs. We consider a standard post-training quantization (PTQ) setting, where each layer f_ℓ is approximated by a quantized counterpart \tilde{f}_ℓ with quantized weights $\tilde{\theta}_\ell$. Since model weights and activations often exhibit imbalanced distributions, such as heavy tails or channel-wise variance disparity, direct quantization is suboptimal because quantization levels are inefficiently allocated over the dynamic range.

To address this, we employ an invertible transformation \mathbf{P}_ℓ to reshape the representation while preserving the original function. For each layer ℓ , the full-precision mapping can be equivalently written as

$$\mathbf{H}_{t,\ell} = (\mathbf{H}_{t,\ell-1} \mathbf{P}_\ell) (\mathbf{W}_\ell \mathbf{P}_\ell^{-\top})^\top. \quad (2)$$

Accordingly, quantized inference is performed as

$$\tilde{\mathbf{H}}_{t,\ell} = Q_a(\tilde{\mathbf{H}}_{t,\ell-1} \mathbf{P}_\ell; c_\ell) Q_w(\mathbf{W}_\ell \mathbf{P}_\ell^{-\top})^\top, \quad \tilde{\mathbf{H}}_{t+1,0} = \tilde{\mathbf{H}}_{t,L}. \quad (3)$$

Here, Q_w and Q_a denote weight and activation quantization, respectively. For an activation element x at layer ℓ , symmetric uniform quantization is defined as

$$Q_a(x; c_\ell) = c_\ell \cdot \text{clip}(\lfloor x/c_\ell \rfloor, q_{\min}, q_{\max}), \quad (4)$$

where c_ℓ determines the spacing between quantization levels, and q_{\min} and q_{\max} denote the minimum and maximum representable integer levels, respectively.

Compared to conventional quantization, quantizing LoopLMs introduces two distinct sources of mismatch: (i) loop-wise variation in activation distributions within each shared layer, where the quantization parameters $(\mathbf{P}_\ell, c_\ell)$ are fixed across loops while activations vary across loops; and (ii) recursive evolution of hidden states, where $\mathbf{H}_{t,\ell}$ changes across loops, leading to compounded distribution shifts that cannot be captured by a single static quantization configuration.

3 Where Quantization Error Arises in LoopLMs

We analyze how the mismatch between static quantization and dynamic hidden-state evolution in LoopLMs leads to two coupled effects. All proofs are provided in Appendix A.

Distribution Shift within Loops. A key challenge arises because the same quantized layer \tilde{f}_ℓ must process loop-dependent hidden states generated by recursive computation.

This mismatch manifests in two forms. First, a shared activation scale c_ℓ cannot fit all loops when activation magnitudes vary: a large c_ℓ reduces resolution for small activations, while a small c_ℓ causes clipping for large activations. Second, a shared transformation \mathbf{P}_ℓ can only align activation geometry over a limited portion of the loop trajectory. As hidden states $\mathbf{H}_{t,\ell}$ evolve, their dominant directions and channel-wise energy distributions shift, producing loop-dependent outlier patterns. Thus, a fixed \mathbf{P}_ℓ may suppress quantization-sensitive directions in some loops but amplify them in others, misaligning quantization noise with critical features.

Proposition 1. Define the transformed activations at layer ℓ as $\hat{\mathbf{H}}_{t,\ell-1} := \mathbf{H}_{t,\ell-1} \mathbf{P}_\ell$. Assume that for each loop t , $\hat{\mathbf{H}}_{t,\ell-1} \sim s_t \mathbf{R}_t$, where $s_t > 0$ is a loop-dependent scale, and \mathbf{R}_t is a zero-mean random matrix with covariance Σ_t . Let $Q_a(\cdot; c_\ell)$ be a symmetric quantizer with clipping parameter c_ℓ . The expected activation quantization error is

$$\varepsilon_{t,\ell} := \mathbb{E} \left[\left\| Q_a(\hat{\mathbf{H}}_{t,\ell-1}; c_\ell) - \hat{\mathbf{H}}_{t,\ell-1} \right\|_F^2 \right].$$

If there exist two loops $t \neq t'$ such that either $s_t \neq s_{t'}$ (scale drift) or $\Sigma_t \neq \Sigma_{t'}$ (covariance drift), then no shared pair $(\mathbf{P}_\ell, c_\ell)$ can be jointly optimal for both $\varepsilon_{t,\ell}$ and $\varepsilon_{t',\ell}$. Consequently, shared calibration incurs strictly positive excess error on at least one loop.

Error Propagation across Loops. Beyond distribution shift, PTQ is particularly fragile in LoopLMs because quantization perturbs the entire recurrent hidden-state trajectory rather than isolated layer computations. Recall that $\mathbf{H}_{t+1} = F(\mathbf{H}_t)$ and $\tilde{\mathbf{H}}_{t+1} = \tilde{F}(\tilde{\mathbf{H}}_t)$ denote the full-precision and quantized recurrences over L layers, respectively. Their mismatch arises from two coupled sources: (i) approximation error introduced within each loop by quantizing the layer mappings, and (ii) state mismatch caused by feeding the quantized hidden state $\tilde{\mathbf{H}}_t$ into subsequent computations instead of its full-precision counterpart \mathbf{H}_t . As a result, quantization error is not incurred independently at each layer or loop, but instead recursively alters future hidden states and compounds along the recurrent trajectory, especially at loop transitions $t \rightarrow t + 1$ (see Fig. 1).

Proposition 2. Define the loop error as $\varepsilon_t := \|\tilde{\mathbf{H}}_t - \mathbf{H}_t\|_F$. Assume that both recurrences start from the same initial state and, for each loop t , the full-precision function F is γ_t -Lipschitz on the segment between $\tilde{\mathbf{H}}_t$ and \mathbf{H}_t . Then $\varepsilon_{t+1} \leq \varepsilon_t^{\text{quant}} + \gamma_t \varepsilon_t$, where $\varepsilon_t^{\text{quant}} := \|\tilde{F}(\tilde{\mathbf{H}}_t) - F(\tilde{\mathbf{H}}_t)\|_F$. Unrolling this recursion yields

$$\varepsilon_T \leq \sum_{\tau=0}^{T-1} \left(\prod_{t=\tau+1}^{T-1} \gamma_t \right) \varepsilon_\tau^{\text{quant}}.$$

Thus, each loop-wise quantization error is propagated through downstream loop sensitivities, with earlier errors passing through a longer chain of transformations.

Takeaway. Accordingly, error accumulation in quantized LoopLMs is governed by the loop-wise quantization error $\varepsilon_t^{\text{quant}}$ and sensitivity γ_t . Since LoopLMs use a shared static quantization configuration across loops, loop-dependent distribution shifts are unavoidable, as shown in Proposition 1. These shifts increase $\varepsilon_t^{\text{quant}}$ and can move hidden states into regimes where $\gamma_t > 1$. Proposition 2 then implies that errors can be multiplicatively amplified across loops rather than merely accumulate linearly.

4 LoopQ: Loop-Aware PTQ for Looped Transformers

As shown in Proposition 2, accumulated quantization error is governed by the within-loop error $\varepsilon_t^{\text{quant}}$ and the cross-loop amplification factor γ_t . This motivates LoopQ to reduce both local quantization mismatch and recurrent error amplification. Starting from a shared transformation-based quantized backbone [24, 35], LoopQ introduces lightweight loop-dependent adaptations for dynamic hidden-state evolution: (i) *Loop-aware Activation Scaling* (LAS) uses loop-dependent activation ranges to reduce scale mismatch at low cost; (ii) *Selective Loop-aware Transformation* (SLT) relaxes shared transformations only for critical modules identified by sharing-gap analysis, reducing geometry mismatch; (iii) the *Cross-loop Transition Adapter* (CTA) aligns the quantized loop output before it becomes the next loop input, limiting cross-loop amplification; and (iv) *Trajectory-Aware Calibration* jointly optimizes LAS, SLT, and CTA under the recurrent dynamics that drive error accumulation.

4.1 Loop-aware Activation Scaling

Sharing quantization parameters, such as \mathbf{P}_ℓ and c_ℓ , across loops creates a key trade-off in LoopLM quantization. Full sharing maximizes reuse and deployment efficiency, but becomes increasingly misaligned as hidden states evolve in scale and direction (Proposition 1). Fully specialized configurations better fit loop-dependent distributions, but introduce substantial memory overhead and weaken recursive efficiency. Thus, LoopQ balances these goals by preserving a shared backbone and adding lightweight loop-dependent parameters only where mismatch is most pronounced.

We begin with the activation scale c_ℓ , which directly controls quantization resolution and dynamic range. Since the same shared module processes loop-dependent hidden states with varying magnitudes, a shared c_ℓ induces an inherent trade-off: ranges suitable for large activations are too coarse for smaller ones, while ranges tuned for small activations cause clipping for larger ones [35, 37]. This misalignment introduces quantization error that propagates across loops, either reducing resolution or

causing irreversible information loss, and accumulates along the recurrent trajectory. To mitigate this effect, LoopQ replaces the shared activation range c_ℓ with loop-dependent scales $c_{t,\ell}$, i.e., $Q_a(x; c_{t,\ell})$.

These additional parameters are negligible compared to the shared backbone, introducing only $O(TL)$ scalars and thus incurring minimal memory and deployment overhead without meaningfully increasing model capacity. While loop-dependent scaling corrects magnitude mismatch, it does not resolve geometry mismatch. Different loop iterations may still favor different activation geometries that a shared transformation \mathbf{P}_ℓ cannot fully capture. Introducing $\mathbf{P}_{t,\ell}$ for all loops is prohibitively expensive, motivating a more selective mechanism, which we develop next.

4.2 Selective Loop-aware Transformation

We next address residual directional mismatch that cannot be resolved by loop-dependent scaling alone. As the shared module assumes different roles across loops, activation distributions become role-dependent. A single shared transform \mathbf{P}_ℓ must therefore fit multiple role-specific regimes, making strict sharing suboptimal when these roles favor incompatible transformations. We therefore seek to identify layers where loop-dependent adaptation is most beneficial.

Specifically, LoopQ employs *sharing-gap analysis* to estimate module-wise sensitivity to shared quantization. For each layer ℓ , we evaluate the effect of introducing loop-dependent transforms $\mathbf{P}_{t,\ell}$ while keeping all other layers shared. This defines a sharing-gap objective that measures the resulting change in the overall loss \mathcal{L} (Sec. 4.4). Layers with a large sharing gap are thus less suitable for strict parameter sharing.¹

However, directly optimizing this objective would require retraining the model under loop-dependent parameterizations, which is computationally prohibitive. We therefore approximate the sharing-gap objective using a tractable surrogate. Let $\mathbf{P}_{t,\ell} = \mathbf{P}_\ell + \Delta_{t,\ell}$ denote the loop-dependent transform at loop t . Expanding \mathcal{L} around \mathbf{P}_ℓ via a second-order Taylor expansion yields

$$\mathcal{L}(\mathbf{P}_{t,\ell}) \approx \mathcal{L}(\mathbf{P}_\ell) + \nabla \mathcal{L}(\mathbf{P}_\ell)^\top \Delta_{t,\ell} + \frac{1}{2} \Delta_{t,\ell}^\top \nabla^2 \mathcal{L}(\mathbf{P}_\ell) \Delta_{t,\ell}. \quad (5)$$

This shows that introducing loop-dependent variation corresponds to a structured perturbation around the shared solution. The first-order term reflects a shift in the optimal shared parameters, which can be partially compensated by adjusting \mathbf{P}_ℓ , while the remaining effect is governed by local curvature. In principle, the sharing-gap objective can be approximated through this second-order expansion.

However, explicitly computing layer-wise Hessians remains impractical for large models. We instead approximate the objective using a proxy based on the inconsistency of gradient directions across loops after curvature normalization [9]. Large variation indicates that different loops favor incompatible updates, making a single shared transform insufficient to capture all loop regimes.

$$S_\ell = \sum_j \frac{\text{Var}_t(\phi_{t,\ell,j})}{\psi_{\ell,j} + \epsilon} \approx \sum_j \frac{\frac{1}{T} \sum_{t=0}^{T-1} \phi_{t,\ell,j}^2 - \left(\frac{1}{T} \sum_{t=0}^{T-1} \phi_{t,\ell,j}\right)^2}{\psi_{\ell,j} + \epsilon}. \quad (6)$$

Here, $\phi_{t,\ell,j}$ denotes the j -th coordinate of the gradient of \mathcal{L} with respect to \mathbf{P}_ℓ at loop t , and $\psi_{\ell,j}$ is the corresponding diagonal Fisher curvature estimate [25]. The constant $\epsilon > 0$ prevents near-zero curvature dimensions from being overestimated. Thus, S_ℓ measures curvature-normalized gradient variance across loops, capturing the inconsistency of update directions under recursive computation and identifying layers less suitable for parameter sharing. Since \mathcal{L} is defined over the recurrent trajectory, this score prioritizes transformations whose shared mismatch has larger downstream effects across loops.

Finally, LoopQ progressively selects sharing-sensitive layers according to S_ℓ . Instead of relying on a one-shot ranking, LoopQ alternates between adapting the selected transformations and re-evaluating S_ℓ , allowing subsequent selections to target complementary residual mismatch. For the selected layers, LoopQ introduces loop-dependent transforms $\mathbf{P}_{t,\ell}$ together with loop-dependent activation ranges $c_{t,\ell}$, while the remaining layers stay fully shared with a single \mathbf{P}_ℓ across loops. This strategy requires loop-dependent adaptation for only about 5% of transformation parameters.

¹Selection is performed at the matrix level rather than the whole-layer level, enabling more fine-grained adaptation.

4.3 Cross-loop Transition Adapter

Even after mitigating layer-level mismatch through loop-dependent scaling and transformation, residual errors can still accumulate at loop transitions due to state reuse. Specifically, the output of one loop is directly fed as the input to the next, allowing quantization-induced distortions to carry forward and amplify across loops. A lightweight correction at this interface can therefore reduce cross-loop error accumulation (Proposition 2) without modifying the shared quantized backbone.

LoopQ introduces a lightweight cross-loop adapter A_t that adjusts the quantized hidden state before it enters loop $t + 1$. The adapted hidden state is computed as $\tilde{\mathbf{H}}_{t+1,0} = A_t(\tilde{\mathbf{H}}_{t,L})$, where

$$A_t(\tilde{\mathbf{H}}_{t,L}) = \tilde{\mathbf{H}}_{t,L} + (\mathbf{a}_t - 1) \odot \text{RMSNorm}(\tilde{\mathbf{H}}_{t,L}) + \mathbf{b}_t + ((\text{RMSNorm}(\tilde{\mathbf{H}}_{t,L})\mathbf{V}) \odot \eta_t)\mathbf{U}^\top. \quad (7)$$

Here, $\text{RMSNorm}(\cdot)$ denotes normalization along the feature dimension [42]. The affine correction rescales each feature by \mathbf{a}_t and shifts it by \mathbf{b}_t , stabilizing activation distributions at loop transitions. The low-rank correction captures structured mismatch beyond this coarse adjustment. The matrices \mathbf{U} and \mathbf{V} are shared across loops to provide reusable correction directions, while only the lightweight loop-dependent parameters $\{\mathbf{a}_t, \mathbf{b}_t, \eta_t\}$ vary with t . The gate η_t modulates the correction strength across loop depth with negligible overhead.

4.4 Trajectory-Aware Calibration

Building on the preceding components, we introduce a trajectory-aware objective that aligns calibration and distillation with loop evolution, enabling shared and loop-dependent parameters to be optimized consistently with the recursive inference process.

To recover performance after quantization, LoopQ performs joint distillation [13] on the calibration set \mathcal{D} using the full-precision model as the reference. The objective is defined as

$$\mathcal{L} = \mathbb{E}_{x \sim \mathcal{D}} \left[\text{KL}(\mathbf{Z} \parallel \tilde{\mathbf{Z}}) + \lambda \left(\sum_{t=0}^{T-1} \left(\|\tilde{\mathbf{H}}_{t,L} - \mathbf{H}_{t,L}\|_2^2 + \|\tilde{\mathbf{H}}_{t,L} - \mathbf{H}_T\|_2^2 \right) + \sum_{t=0}^{T-2} \|A_t(\tilde{\mathbf{H}}_{t,L}) - \mathbf{H}_{t+1,0}\|_2^2 \right) \right] \quad (8)$$

The first term minimizes the KL divergence between the full-precision logits \mathbf{Z} and quantized logits $\tilde{\mathbf{Z}}$, enforcing prediction-level consistency. The trajectory-level terms serve two complementary purposes: (a) aligning $\tilde{\mathbf{H}}_{t,L}$ with $\mathbf{H}_{t,L}$ to preserve loop-wise full-precision hidden states, and (b) encouraging $\tilde{\mathbf{H}}_{t,L}$ to approach the final recurrent state \mathbf{H}_T , consistent with fixed-point convergence [17] in looped Transformers, with further details discussed in Appendix B.4. The transition term regularizes loop-to-loop dynamics by requiring the adapted quantized state $A_t(\tilde{\mathbf{H}}_{t,L})$ to approximate the next-loop input state $\mathbf{H}_{t+1,0}$. Here, λ balances logit-level supervision and trajectory-level matching.

Because LoopLMs recursively reuse hidden states, the input distribution evolves across loops rather than remaining fixed. Since $\mathbf{H}_{t,L}$ depends on states from earlier loops, conventional layer-wise calibration cannot capture cross-loop distribution shifts or error propagation. LoopQ addresses this by jointly optimizing Eq. (8) along the recursive computation path, allowing gradients from later loops to update shared quantized components and earlier loop-dependent adaptations. The optimized parameters include shared transforms \mathbf{P}_ℓ and loop-dependent components: activation ranges $c_{t,\ell}$, selected transforms $\mathbf{P}_{t,\ell}$ identified via sharing-gap analysis, and transition adapters A_t . This jointly corrects distribution shifts and accumulated errors across loops.

5 Experiments

We evaluate LoopQ on representative LoopLMs under standard post-training quantization settings. In the main text, we first describe the experimental setup, compare LoopQ with static quantization baselines, and present component ablation studies. Additional analyses on dynamic-layer selection, calibration size, and loop-extrapolation stability are provided in Appendix C.

5.1 Experimental Setup

Benchmarks. Following prior quantization work, we evaluate LoopQ on a standard suite of downstream and language-modeling benchmarks. For all accuracy-based benchmarks, we report

normalized accuracy (`acc_norm`) whenever available, and otherwise use the standard accuracy reported by the evaluation harness. We report HellaSwag (HS) [41] and WinoGrande (WG) [31] for commonsense reasoning, ARC-Challenge (AC) [4] and MMLU (MM) [12] for language understanding, and OpenAI LAMBADA (LB) [27, 29] for long-context prediction. We further report perplexity on WikiText-2 (WT2) [26] and LAMBADA (OP) [27, 29] to assess generative quality.

Baselines. We compare against *BF16* as the full-precision reference, direct *Symmetric* PTQ as a naive baseline, *QuaRot* [2] with weight rotation, *SpinQuant* [24] with learned rotation, *FlatQuant* [35] with affine flattening, and *SmoothQuant* [37] with offline scaling. We evaluate all methods under both W4A4 and W4A8 settings, corresponding to 4-bit weights with 4-bit or 8-bit activations. All methods share the same backbone, so performance differences reflect quantization robustness rather than additional model capacity.

Backbones. We evaluate LoopQ on four LoopLM backbones from three representative LoopLM architectures, including standard LoopLM *Ouro* [45]: 1.4B with 24 layers over 4 loops and 2.6B with 48 layers over 4 loops; shortcut-modulated *LoopFormer* [17]: 3×8 , with 3 layers over 8 loops; and partial-looped *Parcae* [28]: 370M with 4 looped layers over 8 loops plus 8 non-looped layers.

Implementation. Following standard PTQ practice, we use symmetric uniform post-training quantization with round-to-nearest (RTN). Calibration samples are drawn from the Pile [10], and both weights and activations are quantized group-wise with a group size of 32. For dynamically selected loop-dependent modules, LoopQ adapts only about 5% of the transform parameters $\mathbf{P}_{t,\ell}$. All accuracy results are averaged over 10 runs, with standard deviations below 3%. We use FlatQuant-style Kronecker-decomposed transforms [35] and low-rank matrices \mathbf{U} and \mathbf{V} , resulting in a negligible increase in the total number of parameters. Additional implementation details and deployment-overhead analyses are provided in Appendices B.2 and B.3.

5.2 Main Results

Overall improvement. Table 1 shows that static PTQ baselines are poorly matched to LoopLMs because they use a fixed quantization configuration for loop-dependent hidden states. This limitation is most evident under W4A4, where static methods often become unstable: LoopQ improves mean downstream accuracy by 68.8% and reduces average perplexity by about 87.7% over the strongest static baselines. In particular, static quantization methods frequently degrade sharply on perplexity metrics, especially OP. Since perplexity reflects prediction uncertainty, this degradation suggests that fixed quantization configurations amplify cross-loop errors and lead to less reliable generation. Under W4A8, higher activation precision provides more tolerance, but LoopQ still improves mean downstream accuracy by about 9.8% and reduces average perplexity by about 17.1%.

Task-level behavior. The largest gains appear on LAMBADA-related metrics, including task accuracy LB and perplexity OP. Under W4A4 quantization, LoopQ achieved LB accuracies of 34.9% on LoopFormer and 30.0% on Parcae, while even the strongest static baselines yielded near-zero performance. LoopQ also reduced OP perplexity on LoopFormer and Parcae by approximately 64.5% and 88.3%, respectively. This shows that long-context prediction is especially sensitive to accumulated cross-loop distortion. In contrast, gains are more moderate on WG, AC, and MM, with average W4A4 improvements of about 33.5%, since these short-answer classification-style tasks are less exposed to cumulative prediction errors. This suggests that LoopQ is most beneficial when quantization errors repeatedly propagate through long-context recurrent computation.

Backbone-level robustness. LoopQ brings the largest gains on Ouro, where stronger BF16 performance leaves more recoverable capability under quantization. Averaged over W4A4 and W4A8, LoopQ improves mean downstream accuracy over the strongest static baseline by about 61.8% on Ouro 1.4B and 76.3% on Ouro 2.6B. In contrast, LoopFormer and Parcae have lower full-precision performance, limiting the ceiling for recovery and leading to smaller gains of 7.1% and 12.0%, respectively. This suggests that LoopQ is especially beneficial for stronger LoopLMs, where improved quantization robustness translates more directly into downstream accuracy gains.

5.3 Analysis

Ablation Study. Table 2 ablates the three components of LoopQ on Ouro 1.4B. (i) *w/o LAS* removes loop-aware activation scaling, (ii) *w/o SLT* removes selective loop-aware transformation, and

Table 1: Main results under W4A4 and W4A8. BF16 is repeated across the two quantization groups as the same full-precision reference and is italicized to distinguish it from quantized results.

Model	Method	W4A4								W4A8							
		Tasks \uparrow				Perplexity \downarrow				Tasks \uparrow				Perplexity \downarrow			
		HS	WG	LB	AC	MM	WT2	OP	HS	WG	LB	AC	MM	WT2	OP		
Ouro 1.4B	<i>BF16</i>	<i>0.7159</i>	<i>0.6717</i>	<i>0.6505</i>	<i>0.5256</i>	<i>0.6823</i>	<i>12.03</i>	<i>5.30</i>	<i>0.7159</i>	<i>0.6717</i>	<i>0.6505</i>	<i>0.5256</i>	<i>0.6823</i>	<i>12.03</i>	<i>5.30</i>		
	Symmetric	0.2777	0.4941	0.0033	0.2389	0.2282	1.17e3	8.20e4	0.5022	0.5866	0.3220	0.3745	0.3569	43.89	46.72		
	SmoothQuant	0.2575	0.5170	0.0000	0.2457	0.2499	7.71e4	2.91e7	0.6010	0.5722	0.2851	0.4104	0.2910	33.27	60.21		
	QuaRot	0.2908	0.4972	0.0293	0.2270	0.2366	451.44	1.58e4	0.6817	0.6195	0.5523	0.4983	0.5577	15.27	8.95		
	SpinQuant	0.2914	0.4925	0.0078	0.2210	0.2352	653.78	4.37e4	0.4838	0.5630	0.3647	0.3745	0.3240	27.88	27.61		
	FlatQuant	0.2698	0.4483	0.0000	0.2278	0.2358	1.05e4	4.40e5	0.6511	0.5962	0.4983	0.6336	13.53	6.92			
	LoopQ	0.6582	0.5951	0.5659	0.4881	0.5465	15.81	8.18	0.6954	0.6456	0.6255	0.5145	0.6206	13.29	6.09		
Ouro 2.6B	<i>BF16</i>	<i>0.7636</i>	<i>0.6867</i>	<i>0.7013</i>	<i>0.5802</i>	<i>0.7380</i>	<i>10.51</i>	<i>4.22</i>	<i>0.7636</i>	<i>0.6867</i>	<i>0.7013</i>	<i>0.5802</i>	<i>0.7380</i>	<i>10.51</i>	<i>4.22</i>		
	Symmetric	0.2811	0.5043	0.0361	0.2244	0.2311	962.74	7.81e4	0.5517	0.5777	0.4093	0.3729	0.3386	17.21	22.07		
	SmoothQuant	0.2589	0.5012	0.0000	0.2662	0.2455	9.09e4	2.09e7	0.3219	0.5099	0.0693	0.2363	0.2297	198.38	1.81e3		
	QuaRot	0.2967	0.4964	0.0782	0.2329	0.2307	301.26	3.65e3	0.5389	0.5659	0.4157	0.3874	0.4419	15.78	21.53		
	SpinQuant	0.2805	0.4862	0.0200	0.2193	0.2316	621.14	5.17e4	0.5651	0.5754	0.4611	0.4044	0.4432	15.81	17.26		
	FlatQuant	0.2560	0.4917	0.0000	0.2560	0.2455	3.07e4	1.62e7	0.6393	0.6085	0.3895	0.4309	0.4519	25.51	26.07		
	LoopQ	0.6860	0.6227	0.5680	0.5034	0.5265	15.89	8.17	0.7555	0.6780	0.6837	0.5819	0.7007	11.38	4.47		
LoopFormer 3x8	<i>BF16</i>	<i>0.3218</i>	<i>0.5107</i>	<i>0.3776</i>	<i>0.2457</i>	<i>0.2306</i>	<i>35.62</i>	<i>26.26</i>	<i>0.3218</i>	<i>0.5107</i>	<i>0.3776</i>	<i>0.2457</i>	<i>0.2306</i>	<i>35.62</i>	<i>26.26</i>		
	Symmetric	0.2731	0.4988	0.0016	0.2457	0.2391	1.11e3	3.41e4	0.3156	0.5099	0.3621	0.2389	0.2311	39.00	29.51		
	SmoothQuant	0.2653	0.4972	0.0004	0.2440	0.2418	4.08e3	1.16e5	0.3019	0.5178	0.1296	0.2363	0.2301	113.70	396.20		
	QuaRot	0.3087	0.5264	0.0869	0.2389	0.2295	56.05	290.49	0.3207	0.5209	0.3705	0.2363	0.2303	37.47	29.87		
	SpinQuant	0.2959	0.5051	0.2331	0.2176	0.2301	98.20	88.91	0.3049	0.5146	0.2451	0.2244	0.2291	42.83	92.20		
	FlatQuant	0.2782	0.5170	0.0276	0.2184	0.2318	462.39	5.03e3	0.3186	0.5193	0.3798	0.2338	0.2300	38.25	26.85		
	LoopQ	0.3179	0.5296	0.3487	0.2561	0.2345	37.05	31.59	0.3199	0.5264	0.3743	0.2372	0.2300	36.74	27.53		
Parcae 370M	<i>BF16</i>	<i>0.4409</i>	<i>0.5446</i>	<i>0.3565</i>	<i>0.2910</i>	<i>0.2558</i>	<i>26.98</i>	<i>32.55</i>	<i>0.4409</i>	<i>0.5446</i>	<i>0.3565</i>	<i>0.2910</i>	<i>0.2558</i>	<i>26.98</i>	<i>32.55</i>		
	Symmetric	0.2992	0.5091	0.0097	0.2227	0.2455	797.53	7.26e4	0.3983	0.5130	0.1013	0.2688	0.2447	82.00	645.47		
	SmoothQuant	0.3252	0.4980	0.0833	0.2270	0.2379	489.94	914.59	0.3511	0.5162	0.1310	0.2312	0.2355	162.19	250.89		
	QuaRot	0.3534	0.5146	0.1289	0.2321	0.2349	273.18	454.18	0.4214	0.5272	0.3266	0.2756	0.2334	34.41	45.35		
	SpinQuant	0.3057	0.5185	0.0305	0.2201	0.2354	837.26	8.34e3	0.3765	0.5051	0.1807	0.2568	0.2481	207.42	276.29		
	FlatQuant	0.3191	0.4972	0.0695	0.2278	0.2310	219.36	1.14e3	0.4319	0.5422	0.3278	0.2867	0.2366	28.80	40.05		
	LoopQ	0.4174	0.5214	0.3004	0.2961	0.2346	32.05	53.15	0.4411	0.5454	0.3577	0.2929	0.2441	27.83	34.17		

Table 2: Ablation study of Ouro 1.4B under W4A4 and W4A8.

Variant	W4A4								W4A8							
	HS	WG	LB	AC	MM	WT2	OP	HS	WG	LB	AC	MM	WT2	OP		
w/o LAS	0.2602	0.4949	0.0000	0.2534	0.2295	1.45e5	5.71e6	0.6653	0.6322	0.5804	0.5213	0.5034	14.83	7.53		
w/o SLT	0.6178	0.5738	0.5063	0.4215	0.3774	19.27	12.01	0.6910	0.6433	0.6334	0.5205	0.6107	13.58	6.51		
w/o CTA	0.6567	0.5909	0.5540	0.4812	0.4865	16.33	8.63	0.6940	0.6393	0.6047	0.5316	0.6081	13.46	6.87		
LoopQ	0.6582	0.5951	0.5659	0.4881	0.5465	15.81	8.18	0.6954	0.6456	0.6255	0.5145	0.6206	13.29	6.09		

(iii) *w/o CTA* removes cross-loop state alignment. These variants isolate three sources of recurrent quantization error: loop-dependent range mismatch, residual loop-dependent geometry mismatch, and transition-state drift across repeated passes. Overall, the largest degradation comes from removing LAS: under W4A4, mean downstream accuracy drops by about 56.6%, and OP perplexity increases by more than five orders of magnitude. Removing SLT causes a smaller but still clear degradation, with about a 12.5% drop in mean downstream accuracy and a 46.8% increase in OP perplexity. Removing CTA has the mildest effect, with only about a 3.0% drop in mean downstream accuracy and a 5.5% increase in OP perplexity. Overall, LAS is the most critical component, while SLT and CTA provide complementary gains by correcting residual geometry mismatch and recurrent state drift.

Quantization robustness over trajectories. Table 1 shows that quantized LoopLMs are highly sensitive to trajectory length, defined by the number of layers across loops. On LAMBADA, nearly all state-of-the-art baselines exceed 200 perplexity under W4A4 OP, suggesting that quantization errors are recursively amplified along the loop trajectory rather than remaining local perturbations. To examine this effect, we compare layer-wise ℓ_2 errors across loops on LAMBADA. As shown in Fig. 2, baseline errors quickly diverge and exhibit sharp spikes at loop transitions, where the final-layer output of one loop becomes the input to the next. Comparing Ouro 1.4B (a) with Parcae (b), we observe more severe error accumulation in the model with a longer loop trajectory. Other baselines saturate in the middle loops, suggesting that later hidden states become dominated by quantization noise. In contrast, LoopQ suppresses error accumulation and reduces transition spikes by correcting loop-dependent activation shifts and geometric mismatches. Further analysis in Appendix C shows that these gains mainly come from targeted loop-aware adaptation and trajectory-aware calibration, rather than larger adaptation or calibration budgets.

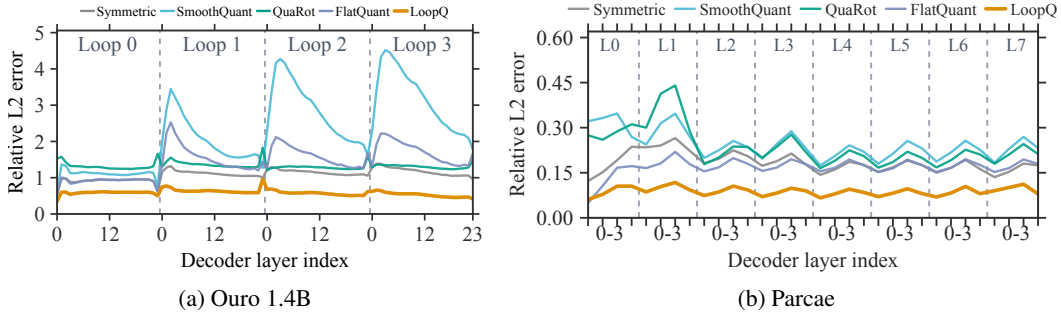


Figure 2: Quantization error across layers and loops on LAMBADA, measured by the relative ℓ_2 norm between quantized and full-precision activations.

6 Related Work

PTQ for LLMs. Post-training quantization (PTQ) [1, 7, 9, 22, 24, 34, 35, 38] reduces the memory footprint and inference cost of LLMs without retraining. Early weight-only methods minimize rounding errors using approximate second-order information [9] or preserve activation-salient channels for low-bit robustness [22], but they provide limited runtime memory reduction because activation memory remains dominant, especially in long-context inference. Joint weight-activation quantization further improves efficiency but makes activation outliers the central challenge, motivating explicit outlier-handling methods that retain extreme dimensions in higher precision [6], allocate bits by salience [15], or preserve high-variance subspaces [33]. Since such strategies may complicate deployment, another line of work reshapes activation distributions to ease quantization, including SmoothQuant [37], which redistributes quantization difficulty through channel-wise scaling; rotation-based methods such as QuaRot [2] and SpinQuant [24], which redistribute channel energy; and geometry-aware methods such as OSTQuant [14], FlatQuant [35], and MixQuant [32], which further improve activation geometry for quantization. However, these methods generally assume static quantization configurations, which are not well aligned with LoopLMs, where parameter sharing induces loop-dependent activation distributions and loop-dependent quantization behavior.

Looped Language Models. Recent parameter-efficient architectures exploit inter-layer redundancy through layer merging [16, 23, 36, 44], which compresses model depth while maintaining performance but still operates in a single forward pass. Looped language models extend this idea by explicitly reusing a shared stack of layers across loops, enabling multi-step computation and adaptive reasoning. Early works such as Universal Transformer [5] and ALBERT [21] demonstrate that parameter sharing improves efficiency with minimal performance degradation, while more recent approaches including Mixture of Recursions [3], Ouro [45], HyperLoop [40], Parcae [28] and LoopFormer [17] explore recursive reasoning and dynamic-depth computation. As LLM inference increasingly becomes memory-bandwidth-bound rather than compute-bound [19, 20, 43], looped architectures are also favorable for hardware–software co-design and memory-constrained deployment, since parameter sharing reduces memory traffic and alleviates bandwidth bottlenecks [11, 30]. However, existing looped-model studies focus primarily on architecture design, parameter efficiency, and full-precision behavior, with limited discussion of low-bit PTQ. In particular, the quantization-specific effects induced by shared recursion, such as loop-dependent activation mismatch and error accumulation across loops, remain underexplored.

7 Conclusion and Limitation

In this paper, we present **LoopQ**, a loop-aware post-training quantization framework for looped Transformers. We show that LoopLMs face unique quantization challenges caused by loop-dependent distribution shifts, transition-state reuse, and recursive error accumulation. LoopQ addresses these challenges by preserving a shared quantized backbone while adding lightweight loop-dependent adaptations, including activation scaling, selective transformation, cross-loop state alignment, and trajectory-aware calibration. Experiments across multiple LoopLM backbones and benchmarks demonstrate that LoopQ consistently improves low-bit robustness over static PTQ baselines, especially under challenging W4A4 quantization. A current limitation of LoopQ is its focus on fixed-path

decoding with a predetermined loop structure, while extensions to dynamic inference, long-context generation, and hardware-aware deployment remain open directions for future work.

References

- [1] M. Alizadeh, A. Behboodi, M. van Baalen, C. Louizos, T. Blankevoort, and M. Welling. Gradient l1 regularization for quantization robustness. In *International Conference on Learning Representations*, 2020.
- [2] S. Ashkboos, A. Mohtashami, M. L. Croci, B. Li, P. Cameron, M. Jaggi, D. Alistarh, T. Hoefler, and J. Hensman. Quarot: Outlier-free 4-bit inference in rotated llms. *Advances in Neural Information Processing Systems*, 37:100213–100240, 2024.
- [3] S. Bae, Y. Kim, R. Bayat, S. Kim, J. Ha, T. Schuster, A. Fisch, H. Harutyunyan, Z. Ji, A. Courville, et al. Mixture-of-recursions: Learning dynamic recursive depths for adaptive token-level computation. *arXiv preprint arXiv:2507.10524*, 2025.
- [4] P. Clark, I. Cowhey, O. Etzioni, T. Khot, A. Sabharwal, C. Schoenick, and O. Tafjord. Think you have solved question answering? try arc, the ai2 reasoning challenge. *arXiv preprint arXiv:1803.05457*, 2018.
- [5] M. Dehghani, S. Gouws, O. Vinyals, J. Uszkoreit, and Ł. Kaiser. Universal transformers. *arXiv preprint arXiv:1807.03819*, 2018.
- [6] T. Dettmers, M. Lewis, Y. Belkada, and L. Zettlemoyer. Gpt3. int8 (): 8-bit matrix multiplication for transformers at scale. *Advances in neural information processing systems*, 35:30318–30332, 2022.
- [7] K. Egashira, M. Vero, R. Staab, J. He, and M. Vechev. Exploiting llm quantization. *Advances in Neural Information Processing Systems*, 37:41709–41732, 2024.
- [8] Y. Fan, Y. Du, K. Ramchandran, and K. Lee. Looped transformers for length generalization. *arXiv preprint arXiv:2409.15647*, 2024.
- [9] E. Frantar, S. Ashkboos, T. Hoefler, and D. Alistarh. Gptq: Accurate post-training quantization for generative pre-trained transformers. *arXiv preprint arXiv:2210.17323*, 2022.
- [10] L. Gao, S. Biderman, S. Black, L. Golding, T. Hoppe, C. Foster, J. Phang, H. He, A. Thite, N. Nabeshima, et al. The pile: An 800gb dataset of diverse text for language modeling. *arXiv preprint arXiv:2101.00027*, 2020.
- [11] N. Gupta, P. Wang, R. Kannan, and V. K. Prasanna. A persistent-state dataflow accelerator for memory-bound linear attention decode on fpga. *arXiv preprint arXiv:2603.05931*, 2026.
- [12] D. Hendrycks, C. Burns, S. Basart, A. Zou, M. Mazeika, D. Song, and J. Steinhardt. Measuring massive multitask language understanding. *arXiv preprint arXiv:2009.03300*, 2020.
- [13] G. Hinton, O. Vinyals, and J. Dean. Distilling the knowledge in a neural network. *arXiv preprint arXiv:1503.02531*, 2015.
- [14] X. Hu, Y. Cheng, D. Yang, Z. Xu, Z. Yuan, J. Yu, C. Xu, Z. Jiang, and S. Zhou. Ostquant: Refining large language model quantization with orthogonal and scaling transformations for better distribution fitting. *arXiv preprint arXiv:2501.13987*, 2025.
- [15] W. Huang, H. Qin, Y. Liu, Y. Li, Q. Liu, X. Liu, L. Benini, M. Magno, S. Zhang, and X. Qi. Slim-llm: Saliency-driven mixed-precision quantization for large language models. *arXiv preprint arXiv:2405.14917*, 2024.
- [16] M. Imfeld, J. Graldi, M. Giordano, T. Hofmann, S. Anagnostidis, and S. P. Singh. Transformer fusion with optimal transport. *arXiv preprint arXiv:2310.05719*, 2023.
- [17] A. Jeddi, M. Ciccone, and B. Taati. Loopformer: Elastic-depth looped transformers for latent reasoning via shortcut modulation. *arXiv preprint arXiv:2602.11451*, 2026.

- [18] J. Kim, Y. J. Park, S. Son, C. Lee, H.-y. Kim, J. Kim, and Y. Jeon. Turboboa: Faster and exact attention-aware quantization without backpropagation. *arXiv preprint arXiv:2602.04929*, 2026.
- [19] H. Kwon, K. Koo, J. Kim, W. Lee, M. Lee, G. Jung, H. Lee, Y. Jung, J. Park, Y. Song, et al. Pimphony: Overcoming bandwidth and capacity inefficiency in pim-based long-context llm inference system. In *2026 IEEE International Symposium on High Performance Computer Architecture (HPCA)*, pages 1–21. IEEE, 2026.
- [20] A. F. Laguna, M. M. Sharifi, A. Kazemi, X. Yin, M. Niemier, and X. S. Hu. Hardware-software co-design of an in-memory transformer network accelerator. *Frontiers in Electronics*, 3:847069, 2022.
- [21] Z. Lan, M. Chen, S. Goodman, K. Gimpel, P. Sharma, and R. Soricut. Albert: A lite bert for self-supervised learning of language representations. *arXiv preprint arXiv:1909.11942*, 2019.
- [22] J. Lin, J. Tang, H. Tang, S. Yang, W.-M. Chen, W.-C. Wang, G. Xiao, X. Dang, C. Gan, and S. Han. Awq: Activation-aware weight quantization for on-device llm compression and acceleration. *Proceedings of machine learning and systems*, 6:87–100, 2024.
- [23] D. Liu, Z. Qin, H. Wang, Z. Yang, Z. Wang, F. Rong, Q. Liu, Y. Hao, B. Li, X. Chen, et al. Pruning via merging: Compressing llms via manifold alignment based layer merging. In *Proceedings of the 2024 Conference on Empirical Methods in Natural Language Processing*, pages 17817–17829, 2024.
- [24] Z. Liu, C. Zhao, I. Fedorov, B. Soran, D. Choudhary, R. Krishnamoorthi, V. Chandra, Y. Tian, and T. Blankevoort. Spinqant: Llm quantization with learned rotations. In *The Thirteenth International Conference on Learning Representations*, 2025.
- [25] J. Martens and R. Grosse. Optimizing neural networks with kronecker-factored approximate curvature. In *International conference on machine learning*, pages 2408–2417. PMLR, 2015.
- [26] S. Merity, C. Xiong, J. Bradbury, and R. Socher. Pointer sentinel mixture models. *arXiv preprint arXiv:1609.07843*, 2016.
- [27] D. Paperno, G. Kruszewski, A. Lazaridou, N.-Q. Pham, R. Bernardi, S. Pezzelle, M. Baroni, G. Boleda, and R. Fernández. The lambda dataset: Word prediction requiring a broad discourse context. In *Proceedings of the 54th annual meeting of the association for computational linguistics (volume 1: Long papers)*, pages 1525–1534, 2016.
- [28] H. Prairie, Z. Novack, T. Berg-Kirkpatrick, and D. Y. Fu. Parcae: Scaling laws for stable looped language models. *arXiv preprint arXiv:2604.12946*, 2026.
- [29] A. Radford, J. Wu, R. Child, D. Luan, D. Amodei, I. Sutskever, et al. Language models are unsupervised multitask learners. *OpenAI blog*, 1(8):9, 2019.
- [30] M. Riera, J. M. Arnau, and A. González. Crew: Computation reuse and efficient weight storage for hardware-accelerated mlps and rnns. *Journal of Systems Architecture*, 129:102604, 2022.
- [31] K. Sakaguchi, R. L. Bras, C. Bhagavatula, and Y. Choi. Winogrande: An adversarial winograd schema challenge at scale. *Communications of the ACM*, 64(9):99–106, 2021.
- [32] S. Sanjeet, I. Colbert, P. Monteagudo-Lago, G. Franco, Y. Umuroglu, and N. J. Fraser. Mixquant: Pushing the limits of block rotations in post-training quantization. *arXiv preprint arXiv:2601.22347*, 2026.
- [33] U. Saxena, S. Sharify, K. Roy, and X. Wang. Resq: Mixed-precision quantization of large language models with low-rank residuals. In *International Conference on Machine Learning*, pages 53095–53114. PMLR, 2025.
- [34] M. Shkolnik, B. Chmiel, R. Banner, G. Shomron, Y. Nahshan, A. Bronstein, and U. Weiser. Robust quantization: one model to rule them all. In *Proceedings of the 34th International Conference on Neural Information Processing Systems*, pages 5308–5317, 2020.

- [35] Y. Sun, R. Liu, H. Bai, H. Bao, K. Zhao, Y. Li, J. Hu, X. Yu, L. Hou, C. Yuan, et al. Flatquant: Flatness matters for llm quantization. In *International Conference on Machine Learning*, pages 57587–57613. PMLR, 2025.
- [36] N. Verma, K. Murray, and K. Duh. Merging feed-forward sublayers for compressed transformers. *arXiv preprint arXiv:2501.06126*, 2025.
- [37] G. Xiao, J. Lin, M. Seznec, H. Wu, J. Demouth, and S. Han. Smoothquant: Accurate and efficient post-training quantization for large language models. In *International conference on machine learning*, pages 38087–38099. PMLR, 2023.
- [38] Y. Xiao, A. Liu, T. Zhang, H. Qin, J. Guo, and X. Liu. Robustmq: benchmarking robustness of quantized models. *Visual Intelligence*, 1(1):30, 2023.
- [39] Z. Yu, Z. Wang, Y. Li, R. Gao, X. Zhou, S. R. Bommurthy, Y. Zhao, and Y. Lin. Edge-llm: Enabling efficient large language model adaptation on edge devices via unified compression and adaptive layer voting. In *Proceedings of the 61st ACM/IEEE Design Automation Conference*, pages 1–6, 2024.
- [40] A. Zeitoun, L. Torroba-Hennigen, and Y. Kim. Hyperloop transformers. *arXiv preprint arXiv:2604.21254*, 2026.
- [41] R. Zellers, A. Holtzman, Y. Bisk, A. Farhadi, and Y. Choi. Hellaswag: Can a machine really finish your sentence? In *Proceedings of the 57th annual meeting of the association for computational linguistics*, pages 4791–4800, 2019.
- [42] B. Zhang and R. Sennrich. Root mean square layer normalization. *Advances in neural information processing systems*, 32, 2019.
- [43] M. Zhou, W. Xu, J. Kang, and T. Rosing. Transpim: A memory-based acceleration via software-hardware co-design for transformer. In *2022 IEEE International Symposium on High-Performance Computer Architecture (HPCA)*, pages 1071–1085. IEEE, 2022.
- [44] W. Zhou, R. Le Bras, and Y. Choi. Modular transformers: Compressing transformers into modularized layers for flexible efficient inference. In *Findings of the Association for Computational Linguistics: ACL 2023*, pages 10452–10465, 2023.
- [45] R.-J. Zhu, Z. Wang, K. Hua, T. Zhang, Z. Li, H. Que, B. Wei, Z. Wen, F. Yin, H. Xing, et al. Scaling latent reasoning via looped language models. *arXiv preprint arXiv:2510.25741*, 2025.

A Detailed Proof

A.1 Notation Table

Table 3: Summary of notations.

Category	Notation	Description
LoopLM	\mathbf{X}	Input token sequence.
	T, L	Number of recursive loops and number of layers in the shared Transformer stack.
	t, ℓ	Loop index and layer index.
	$f_\ell(\cdot; \theta_\ell)$	The ℓ -th full-precision Transformer layer.
	$\mathbf{H}_{t,\ell}$	Hidden state at layer ℓ in loop t .
	\mathbf{H}_t	Input state of loop t , defined as $\mathbf{H}_t := \mathbf{H}_{t,0}$.
	F	One full loop pass through the shared stack, defined as $F := f_L \circ \dots \circ f_1$.
	\mathbf{Z}	Full-precision output logits, $\mathbf{Z} = \text{Proj}(\mathbf{H}_T)$.
PTQ	\mathbf{W}_ℓ	Weight matrix of layer ℓ .
	\mathbf{P}_ℓ	Shared invertible transformation before quantization.
	$\hat{\mathbf{H}}_{t,\ell-1}$	Transformed activation, defined as $\hat{\mathbf{H}}_{t,\ell-1} := \mathbf{H}_{t,\ell-1} \mathbf{P}_\ell$.
	$Q_w(\cdot), Q_a(\cdot)$	Weight and activation quantization functions.
	c_ℓ	Shared activation quantization scale.
	q_{\min}, q_{\max}	Minimum and maximum representable integer levels.
	$\tilde{f}_\ell, \tilde{\theta}_\ell$	Quantized layer and its quantized parameters.
	$\tilde{\mathbf{H}}_{t,\ell}, \tilde{\mathbf{Z}}$	Quantized hidden state and quantized output logits.
Error	ε_t	Loop-level state error, defined as $\varepsilon_t := \ \tilde{\mathbf{H}}_t - \mathbf{H}_t\ _F$.
	$\varepsilon_t^{\text{quant}}$	Quantization error introduced within loop t .
	γ_t	Loop sensitivity factor of the full-precision loop function F .
LoopQ	$c_{t,\ell}$	Loop-dependent activation scale used in Loop-aware Activation Scaling.
	$\mathbf{P}_{t,\ell}$	Loop-dependent transformation used in selected layers.
	S_ℓ	Sharing-gap score for selecting loop-sensitive transformations.
	$A_t(\cdot)$	Cross-loop transition adapter between loop t and loop $t + 1$.
	$\mathbf{a}_t, \mathbf{b}_t, \eta_t$	Loop-dependent parameters in the transition adapter.
	\mathbf{U}, \mathbf{V}	Shared low-rank matrices in the transition adapter.
Calibration	\mathcal{D}	Calibration dataset.
	\mathcal{L}	Trajectory-aware calibration loss.
	$\text{KL}(\cdot \ \cdot)$	Kullback–Leibler divergence for logit distillation.
	λ, α_t	Loss-balancing weight and loop-dependent calibration weight.

A.2 Proof of Proposition 1

Proposition 1. Define the transformed activations at layer ℓ as $\hat{\mathbf{H}}_{t,\ell-1} := \mathbf{H}_{t,\ell-1} \mathbf{P}_\ell$. Assume that for each loop t , $\hat{\mathbf{H}}_{t,\ell-1} \sim s_t \mathbf{R}_t$, where $s_t > 0$ is a loop-dependent scale, and \mathbf{R}_t is a zero-mean random matrix with covariance Σ_t . Let $Q_a(\cdot; c_\ell)$ be a symmetric quantizer with clipping parameter c_ℓ . The expected activation quantization error is

$$\varepsilon_{t,\ell} := \mathbb{E} \left[\left\| Q_a(\hat{\mathbf{H}}_{t,\ell-1}; c_\ell) - \hat{\mathbf{H}}_{t,\ell-1} \right\|_F^2 \right].$$

If there exist two loops $t \neq t'$ such that either $s_t \neq s_{t'}$ (scale drift) or $\Sigma_t \neq \Sigma_{t'}$ (covariance drift), then no shared pair $(\mathbf{P}_\ell, c_\ell)$ can be jointly optimal for both $\varepsilon_{t,\ell}$ and $\varepsilon_{t',\ell}$. Consequently, shared calibration incurs strictly positive excess error on at least one loop.

Proof. We prove the claim by contradiction.

Let the transformed activations at layer ℓ be

$$\hat{\mathbf{H}}_{t,\ell-1} = \mathbf{H}_{t,\ell-1} \mathbf{P}_\ell.$$

The loop-wise activation quantization error is

$$\varepsilon_{t,\ell}(\mathbf{P}_\ell, c_\ell) = \mathbb{E} \left[\left\| Q_a(\hat{\mathbf{H}}_{t,\ell-1}; c_\ell) - \hat{\mathbf{H}}_{t,\ell-1} \right\|_F^2 \right].$$

We first consider scale drift. Assume that, for a fixed shared transformation \mathbf{P}_ℓ , the transformed activations satisfy

$$\hat{\mathbf{H}}_{t,\ell-1} \sim s_t \mathbf{R}_t,$$

where $s_t > 0$ is a loop-dependent scale. Then

$$\varepsilon_{t,\ell}(\mathbf{P}_\ell, c_\ell) = \mathbb{E} \left[\|Q_a(s_t \mathbf{R}_t; c_\ell) - s_t \mathbf{R}_t\|_F^2 \right].$$

For a symmetric clipping-based uniform quantizer, the quantization map is positively homogeneous:

$$Q_a(s\mathbf{X}; c) = s Q_a(\mathbf{X}; c/s), \quad s > 0.$$

Therefore,

$$\varepsilon_{t,\ell}(\mathbf{P}_\ell, c_\ell) = s_t^2 \mathbb{E} \left[\|Q_a(\mathbf{R}_t; c_\ell/s_t) - \mathbf{R}_t\|_F^2 \right] = s_t^2 \varphi_t(\mathbf{P}_\ell, \alpha_t),$$

where

$$\alpha_t := c_\ell/s_t.$$

Thus, for a fixed \mathbf{P}_ℓ , optimizing c_ℓ for loop t is equivalent to optimizing the normalized clipping ratio α_t .

Assume that the normalized objective $\varphi_t(\mathbf{P}_\ell, \alpha)$ has a unique minimizer $\alpha_t^*(\mathbf{P}_\ell)$. Then the optimal clipping value for loop t is

$$c_{t,\ell}^*(\mathbf{P}_\ell) = s_t \alpha_t^*(\mathbf{P}_\ell).$$

If a shared clipping value c_ℓ were simultaneously optimal for two loops $t \neq t'$, then it must satisfy

$$c_\ell = s_t \alpha_t^*(\mathbf{P}_\ell) = s_{t'} \alpha_{t'}^*(\mathbf{P}_\ell).$$

In particular, when the normalized quantization objectives share the same optimal ratio,

$$\alpha_t^*(\mathbf{P}_\ell) = \alpha_{t'}^*(\mathbf{P}_\ell),$$

the above equality implies $s_t = s_{t'}$, contradicting the scale-drift condition $s_t \neq s_{t'}$. Hence, under scale drift, a shared clipping parameter cannot be simultaneously optimal for both loops.

We next consider directional mismatch. For this part, we analyze the alignment component of \mathbf{P}_ℓ and assume it is constrained to be orthogonal. This captures the common case where the transformation aligns activation directions without changing Euclidean norms. Since

$$\hat{\mathbf{H}}_{t,\ell-1} \sim s_t \mathbf{R}_t, \quad \text{Cov}(\mathbf{R}_t) = \Sigma_t,$$

the second-order geometry observed by a coordinate-wise quantizer is determined by the covariance of the transformed activations. An optimal orthogonal transformation should align the principal activation directions with the quantization axes. A necessary condition is therefore

$$\mathbf{P}_\ell^\top \Sigma_t \mathbf{P}_\ell \text{ is diagonal.}$$

If the same \mathbf{P}_ℓ were also optimal for another loop t' , then we would also require

$$\mathbf{P}_\ell^\top \Sigma_{t'} \mathbf{P}_\ell \text{ is diagonal.}$$

Thus, a shared optimal transformation would require Σ_t and $\Sigma_{t'}$ to be simultaneously orthogonally diagonalizable.

For symmetric covariance matrices, simultaneous orthogonal diagonalizability is equivalent to commutativity. Therefore, if

$$\Sigma_t \Sigma_{t'} \neq \Sigma_{t'} \Sigma_t,$$

then no shared orthogonal transformation \mathbf{P}_ℓ can diagonalize both covariance matrices. This contradicts the assumption that a single shared transformation can be simultaneously optimal for both loops.

Combining the two cases, scale drift makes the optimal clipping parameter loop-dependent, while covariance drift makes the optimal alignment transformation loop-dependent. Hence, under either source of drift, there exists no shared configuration $(\mathbf{P}_\ell, c_\ell)$ that simultaneously minimizes $\varepsilon_{t,\ell}$ and $\varepsilon_{t',\ell}$.

Finally, let $(\mathbf{P}_{t,\ell}^*, c_{t,\ell}^*)$ and $(\mathbf{P}_{t',\ell}^*, c_{t',\ell}^*)$ denote loop-wise minimizers. Since no shared pair can coincide with both loop-wise optima, any shared calibration $(\mathbf{P}_\ell, c_\ell)$ must satisfy

$$\varepsilon_{t,\ell}(\mathbf{P}_\ell, c_\ell) > \varepsilon_{t,\ell}(\mathbf{P}_{t,\ell}^*, c_{t,\ell}^*)$$

or

$$\varepsilon_{t',\ell}(\mathbf{P}_\ell, c_\ell) > \varepsilon_{t',\ell}(\mathbf{P}_{t',\ell}^*, c_{t',\ell}^*).$$

Therefore, shared calibration incurs strictly positive excess error on at least one loop. The proposition follows. \square

A.3 Proof of Proposition 2

Proposition 2. Define the loop error as $\varepsilon_t := \|\tilde{\mathbf{H}}_t - \mathbf{H}_t\|_F$. Assume that both recurrences start from the same initial state and, for each loop t , the full-precision function F is γ_t -Lipschitz on the segment between $\tilde{\mathbf{H}}_t$ and \mathbf{H}_t . Then $\varepsilon_{t+1} \leq \varepsilon_t^{\text{quant}} + \gamma_t \varepsilon_t$, where $\varepsilon_t^{\text{quant}} := \|\tilde{F}(\tilde{\mathbf{H}}_t) - F(\tilde{\mathbf{H}}_t)\|_F$. Unrolling this recursion yields

$$\varepsilon_T \leq \sum_{\tau=0}^{T-1} \left(\prod_{t=\tau+1}^{T-1} \gamma_t \right) \varepsilon_\tau^{\text{quant}}.$$

Thus, each loop-wise quantization error is propagated through downstream loop sensitivities, with earlier errors passing through a longer chain of transformations.

Proof. By definition,

$$\varepsilon_{t+1} = \|\tilde{\mathbf{H}}_{t+1} - \mathbf{H}_{t+1}\|_F = \|\tilde{F}(\tilde{\mathbf{H}}_t) - F(\mathbf{H}_t)\|_F.$$

Applying the triangle inequality gives

$$\varepsilon_{t+1} \leq \|\tilde{F}(\tilde{\mathbf{H}}_t) - F(\tilde{\mathbf{H}}_t)\|_F + \|F(\tilde{\mathbf{H}}_t) - F(\mathbf{H}_t)\|_F.$$

By the definition of the loop-wise quantization error,

$$\|\tilde{F}(\tilde{\mathbf{H}}_t) - F(\tilde{\mathbf{H}}_t)\|_F = \varepsilon_t^{\text{quant}}.$$

Since F is γ_t -Lipschitz on the segment between $\tilde{\mathbf{H}}_t$ and \mathbf{H}_t , we have

$$\|F(\tilde{\mathbf{H}}_t) - F(\mathbf{H}_t)\|_F \leq \gamma_t \|\tilde{\mathbf{H}}_t - \mathbf{H}_t\|_F = \gamma_t \varepsilon_t.$$

Combining the two bounds yields

$$\varepsilon_{t+1} \leq \varepsilon_t^{\text{quant}} + \gamma_t \varepsilon_t.$$

Unrolling this recursion from 0 to $T - 1$ gives

$$\varepsilon_T \leq \left(\prod_{t=0}^{T-1} \gamma_t \right) \varepsilon_0 + \sum_{\tau=0}^{T-1} \left(\prod_{t=\tau+1}^{T-1} \gamma_t \right) \varepsilon_\tau^{\text{quant}},$$

where the empty product is defined as 1. Since the full-precision and quantized recurrences start from the same initial state, $\tilde{\mathbf{H}}_0 = \mathbf{H}_0$, we have $\varepsilon_0 = 0$. Therefore,

$$\varepsilon_T \leq \sum_{\tau=0}^{T-1} \left(\prod_{t=\tau+1}^{T-1} \gamma_t \right) \varepsilon_\tau^{\text{quant}}.$$

Thus, the quantization error introduced at loop τ is propagated through all downstream sensitivity factors $\gamma_{\tau+1}, \dots, \gamma_{T-1}$. Earlier errors pass through a longer chain of loop transformations and can therefore have a larger effect on the final state. The proposition follows. \square

B Detailed Experimental Setup

B.1 Loop-dependent Module Selection.

To preserve the coupling between each transformation and the linear weights that consume its transformed activations, selection is performed at the level of transform–weight groups. Each group is the minimum selectable unit in our implementation and consists of a transformation module together with the quantized linear weights applied to its output activations. The candidate set is constructed directly in this grouped form, and the scores of all linear layers within each group are aggregated to estimate group-level importance. Unselected groups retain the shared transform and shared quantized weights, while selected groups use loop-dependent versions of both components. The detailed grouping strategy is shown in Table 4.

Table 4: Transform-weight groups used as the minimum units for dynamic loop-dependent selection.

Model	Candidate group	Weight side	Transform side
Ouro	self_attn.qkv_proj	q_proj, k_proj, v_proj	self_attn.ln_trans
	self_attn.o_proj	o_proj	self_attn.o_trans
	mlp.up_gate	gate_proj, up_proj	mlp.up_gate_trans
	mlp.down_proj	down_proj	mlp.down_trans
LoopFormer	attn.qkv	attn.c_attn	attn.in_trans
	attn.out	attn.c_proj	attn.out_trans
	mlp.up	mlp.c_fc	mlp.up_trans
	mlp.down	mlp.c_proj	mlp.down_trans
Parcae	attn.qkv	attn.c_q, attn.c_k, attn.c_v	attn.in_trans
	attn.out	attn.c_proj	attn.out_trans
	mlp.up	mlp.fc	mlp.up_trans
	mlp.down	mlp.proj	mlp.down_trans

Table 5: Parameter overhead and memory footprint summary. **Shared** denotes quantization parameters shared across all loops, while **Loop-Dep.** denotes additional loop-dependent parameters used for dynamic loop-wise adaptation during deployment. **Memory footprint** is reported in GB.

Model	Total Params	Shared		Loop-Dep.		Memory Footprint		
		Params	Ratio	Params	Ratio	BF16	LoopQ W4A4	Rel.
Ouro 1.4B	1.476B	40.65M	2.75%	649.5K	0.044%	2.672	1.147	-57.1%
Ouro 2.6B	2.750B	82.16M	2.99%	293.6K	0.0107%	4.969	1.902	-61.7%
LoopFormer 3×8	282.19M	3.69M	1.31%	328.0K	0.116%	0.5240	0.3808	-27.3%
Parcae 370M	390.27M	1.70M	0.44%	304.8K	0.078%	0.7237	0.5190	-28.3%

B.2 Deployment Overhead

We summarize both the parameter overhead and practical loaded memory footprint of LoopQ in Table 5.

Parameter Overhead. Most additional parameters introduced by LoopQ come from the Kronecker-decomposed transformation matrices used in the FlatQuant-style transformation parameterization, making the shared quantization parameters comparable in scale to those introduced by FlatQuant. In contrast, the truly loop-dependent components, including dynamic activation scales and selected loop-dependent transforms, account for only a negligible fraction of the total model parameters, typically at the level of a few hundred thousand parameters and less than 0.12% of the deployed model size.

Memory Footprint. In terms of memory, the reported footprint reflects the actual model state after loading, including packed 4-bit weights, quantization metadata, non-quantized components, and lightweight dynamic loop-dependent parameters. Across all evaluated backbones, LoopQ W4A4 reduces memory relative to the BF16 baseline, achieving reductions of 57.1%, 61.7%, 27.3%, and 28.3% on Ouro 1.4B, Ouro 2.6B, LoopFormer 3×8, and Parcae 370M, respectively. These results indicate that LoopQ preserves the parameter-sharing and deployment advantages of looped models while adding only minimal loop-aware adaptation overhead.

B.3 Implementation Details

Environments. All experiment are conducted on a workstation equipped with an NVIDIA GeForce RTX 5090 GPU with 32GB of memory and an AMD Ryzen 9 9950X CPU. The software stack uses PyTorch 2.9.0 with CUDA 12.8. The GPU hours required for a single calibration run vary by model size but do not exceed 5 hours. Full LM-evaluation runs are performed from the exported artifacts on the same machine, using BF16 model loading together with the quantized runtime kernels.

Quantization Implementation. All experiments use symmetric round-to-nearest post-training quantization (PTQ), with the base models loaded in BF16. Unless otherwise specified, we keep the LM head, token embeddings, position embeddings, and architecture-specific time or modulation

Table 6: Hyperparameters used in experiments.

Hyperparameter	Value
Activation Granularity	Group-wise
Group size	32
Calibration samples	1024
Maximum sequence length	256
LAS activation scales	Per module, per loop
SLT selection budget for Ouro 1.4B	4
SLT selection budget for Ouro 2.6B	8
SLT selection budget for LoopFormer	1
SLT selection budget for Parcae	1
CTA adapter rank	8
λ	0.1
KL temperature	1
Teacher top- k logits	1000
Gradient clipping	1.0

modules unquantized. The calibration set consists of 1,024 samples drawn from the validation split of mit-han-lab/pile-val-backup, using the text column. Detailed hyperparameter settings are presented in Table 6.

B.4 Adaptive weighting for the final teacher target

Recall that the trajectory-aware distillation loss in Eq. (8) uses hidden-state supervision to align the quantized recurrent trajectory with the full-precision teacher trajectory. In particular, the loop-wise target $\mathbf{H}_{t,L}$ preserves the full-precision state at the same loop, while the final target \mathbf{H}_T provides a convergence signal for the quantized state. However, using a fixed relative strength for these two targets can be suboptimal. When the quantized trajectory closely follows the teacher trajectory, the final state \mathbf{H}_T gives useful fixed-point-style guidance. In contrast, when quantization errors introduce a large trajectory mismatch, forcing $\tilde{\mathbf{H}}_{t,L}$ too strongly toward \mathbf{H}_T may over-constrain the quantized recurrence. To balance these effects, we introduce an adaptive weight μ_t to interpolate between the loop-wise teacher target and the final teacher target, and use the following objective in practice:

$$\mathcal{L} = \mathbb{E}_{x \sim \mathcal{D}} \left[\text{KL}(\mathbf{Z} \parallel \tilde{\mathbf{Z}}) + \lambda \left(\sum_{t=0}^{T-1} \left((1 - \mu_t) \|\tilde{\mathbf{H}}_{t,L} - \mathbf{H}_{t,L}\|_2^2 + \mu_t \|\tilde{\mathbf{H}}_{t,L} - \mathbf{H}_T\|_2^2 \right) + \sum_{t=0}^{T-2} \|A_t(\tilde{\mathbf{H}}_{t,L}) - \mathbf{H}_{t+1,0}\|_2^2 \right) \right],$$

where

$$\mu_t = \frac{\|\mathbf{H}_T - \mathbf{H}_{t,L}\|_2^2}{\|\mathbf{H}_T - \mathbf{H}_{t,L}\|_2^2 + \sum_{t'=t}^{T-1} \|\mathbf{H}_{t',L} - \tilde{\mathbf{H}}_{t',L}\|_2^2 + \epsilon}.$$

The numerator measures the remaining distance between the full-precision state at loop t and the final teacher state. When this distance is large, the final state still provides a meaningful convergence direction, so the objective assigns more weight to the final-target supervision. The summation term in the denominator measures the accumulated mismatch between the full-precision and quantized trajectories from loop t onward. When this mismatch becomes large, μ_t decreases, shifting the supervision back toward the loop-wise teacher state and avoiding overly aggressive correction toward \mathbf{H}_T .

Overall, μ_t acts as an adaptive trust weight for final-state guidance. It strengthens the fixed-point-style signal from \mathbf{H}_T when the quantized trajectory remains reliable, and weakens this signal when quantization-induced trajectory mismatch becomes dominant. In practice, μ_t is updated periodically, e.g., every 100 calibration steps, to reduce additional computation and avoid noisy step-wise fluctuations.

C Detailed Analysis of LoopQ

C.1 Loop-dependent Linear Layer Selection

Figure 3 shows that dynamic loop-dependent selection concentrates the adaptation budget on a small set of critical modules rather than distributing it uniformly. The first scan selects the first QKV group,

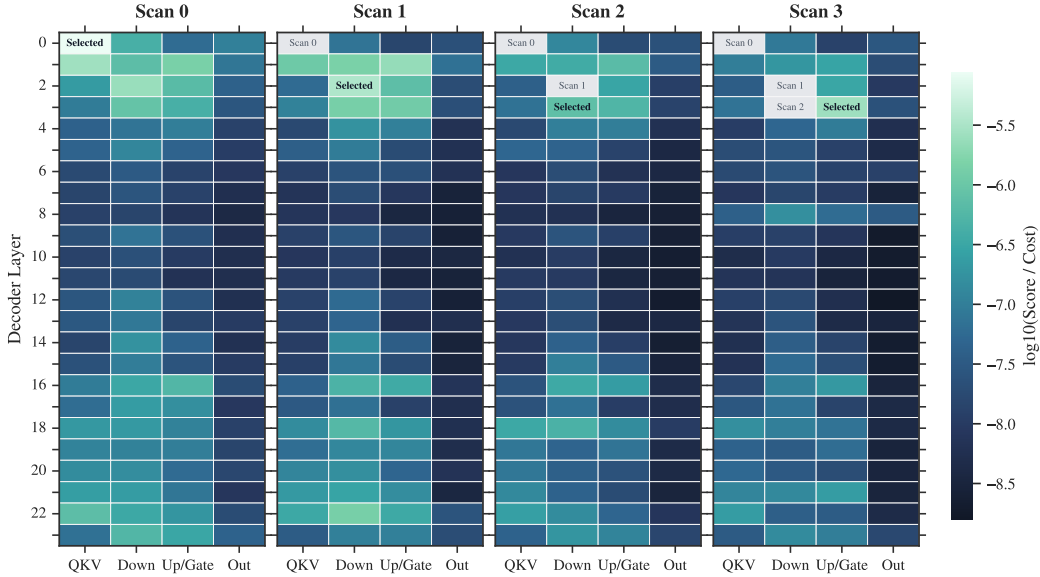


Figure 3: Loop-dependent selection heatmap on Ouro 1.4B.

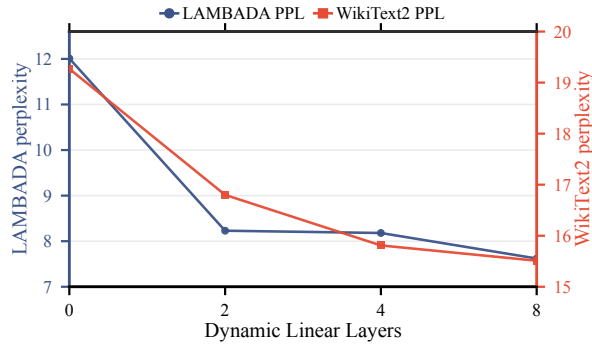


Figure 4: Perplexity under different numbers of selected loop-dependent linear layers.

which is consistent with LoopQ’s motivation: QKV is the input side of attention and directly projects the current-loop hidden state into queries, keys, and values. In looped models, this module is reused under different roles across loops, from embedding-level representations in early passes to refined hidden states in later passes. Thus, activation-scale and geometry mismatch first become exposed at QKV, where a single shared transform may fail to serve multiple loop-dependent regimes.

Subsequent selections of early MLP down and up/gate modules further suggest that LoopQ progressively compensates for residual mismatch propagated through the FFN and residual write-back paths. Overall, this supports the design of preserving a shared quantized backbone while introducing minimal loop-dependent adaptations only for modules that are less suitable for strict sharing.

The heatmap also shows that loop-dependent sensitivity is strongest near the head and tail of the model, while the middle recurrent region is less sensitive. This pattern is consistent with our hypothesis that quantization error in LoopLMs is dominated by role transitions and recurrent interfaces, allowing most modules to remain shared without loop-dependent adaptation.

Figure 4 shows how the number of selected loop-dependent linear layers affects model perplexity. As the number of adapted layers increases from 0 to 2, 4, and 8, perplexity on both LAMBADA and WikiText-2 consistently decreases, demonstrating the benefit of additional loop-dependent flexibility. These adapted layers better capture activation geometry and quantization-error patterns under different loop roles. However, most of the improvement comes from the first few selected layers, with only marginal gains when increasing the budget to 8 layers. This indicates that a small set of high sharing-gap modules accounts for the dominant mismatch. Adding more loop-dependent layers can further

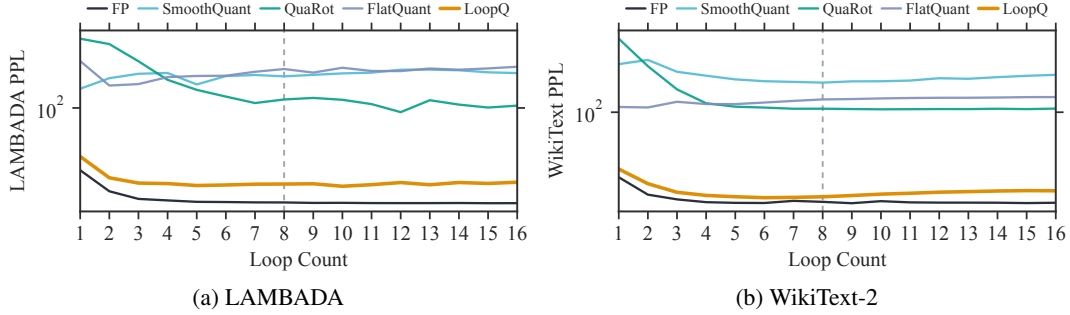


Figure 5: Perplexity under different loop depths.

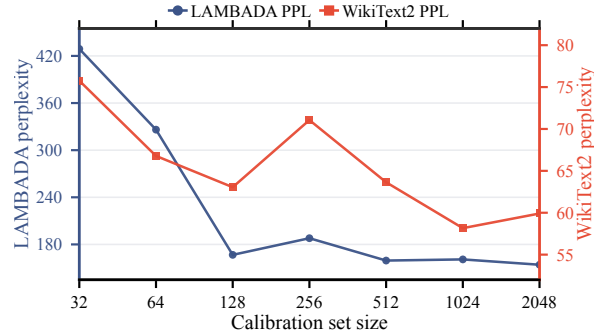


Figure 6: Perplexity under different calibration set sizes.

improve flexibility, but also introduces additional parameters and deployment overhead, creating a trade-off between accuracy recovery and the simplicity of a shared quantized backbone.

C.2 Stability under Loop Extrapolation

Recent studies on looped architectures view recursion as an orthogonal scaling axis that increases inference FLOPs without increasing parameter count [8, 17, 28, 45]. Thus, stability across loop budgets tests whether quantization preserves the model’s original recursive dynamics. Figures 5a and 5b show that, under W4A4 quantization, LoopQ substantially outperforms static baselines on both LAMBADA and WikiText-2. Static baselines maintain PPL values several times larger than the full-precision reference from 8 to 16 loops, whereas LoopQ closely tracks the FP curve and preserves a similar test-time scaling pattern: performance first improves as the loop budget increases and then enters a plateau.

Notably, LoopQ is calibrated only within an 8-loop horizon. When extrapolated to 9–16 loops by extending the trajectory of loop-dependent activation scales, the quantized model does not exhibit mismatch-induced PPL explosion or performance collapse. This suggests that LoopQ not only recovers quantization accuracy at a fixed inference depth but also preserves Parcae’s ability to realize test-time scaling through stable recurrent states. As a result, quantized Parcae remains stable and usable when using intermediate loop outputs or extrapolating to larger loop budgets.

C.3 Calibration-Size Sensitivity Analysis

Figure 6 analyzes the effect of calibration set size. When the number of calibration samples increases from 32 to 128, perplexity on both LAMBADA and WikiText-2 drops substantially, showing that a small calibration set is insufficient to cover distributional variation along the loop trajectory and may lead to unstable quantization and distillation estimates. Beyond 128 samples, however, performance largely saturates with only minor fluctuations. This indicates that LoopQ is not highly sensitive to calibration size once the calibration data covers the major activation distributions, loop-role shifts, and transition states. Further increasing the data size does not provide consistent additional gains, suggesting that LoopQ’s robustness mainly comes from loop-aware selection and trajectory-aware calibration rather than simply using more calibration samples.